IEEE Sensors Council IEEE SENSORS JOURNAL, VOL. XX, NO. XX, MONTH X, XXXX

AC Series Arc Fault Detection Based on RLC Arc Model and Convolutional Neural Network

Run Jiang, Yilong Wang, Xiaoqing Gao, Guanghai Bao, Qiteng Hong and Campbell D. Booth

***Abstract*—AC series arc faults in the power system can lead to electrical fires. However, the generalization performance of the determined detection method would be affected under unknown loads, as current features vary with loads. To address this issue, this paper presents a series arc fault detection method based on a high-frequency (HF) RLC arc model and one-dimensional convolutional neural network (1DCNN). By the current transformer used for receiving differential HF features (D-HFCT), current with complex features is firstly simplified and divided into different oscillation-signal types. Since the types of real D-HFCT data are limited, the RLC arc model is used to generate D-HFCT data with various types of oscillation features by adjusting load types, initial phase angles and Bernoulli-sequence frequencies. Then, the simulated data are adopted to train the 1DCNN model. Finally, the trained 1DCNN model can detect series arc faults under different types of real loads. Compared with the 1DCNN method driven by the limited types of real-current data, the presented method shows good generalization ability and achieves 99.33% average detection accuracy under nine types of unknown loads, which benefits from the training of simulated D-HFCT data with abundant HF oscillation features.**

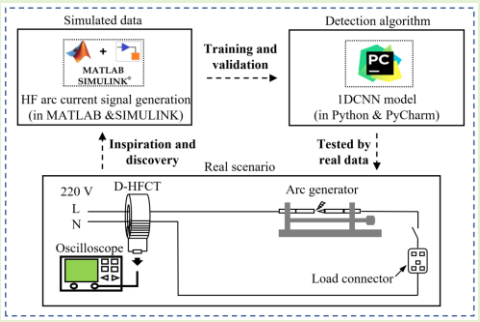

***Index Terms*—AC series arc faults, fault detection, HF oscillation features, 1DCNN, RLC-based arc model.**

I. Introduction

SERIES arc faults are a phenomenon in which electrical discharge occurs in series with the wires. They tend to be caused by loose connection and poor conductivity. The temperature of series arc faults can reach thousands of degrees Celsius, usually accompanied by molten metal [1]. The high temperature probably leads to serious fire and explosion if there are flammable and explosive materials near the fault point. However, the presence of the arc impedance makes the effective value of arcing current lower than that of normal current [2]. Therefore, it is difficult for conventional over-current protection devices to detect series arc faults [3].

To effectively detect series arc faults, various types of detection methods based on data processing and classification have been proposed. Among these recently published methods, time-domain analysis, frequency-domain analysis, time-and-frequency-domain analysis and artificial-intelligence algorithms are commonly used in the field of series arc fault detection.

Since series arc faults can produce obvious distortions in current, the current-based detection is the most popular. According to the time-domain features of current signals, some detection methods which adopt shoulder length, change rate, and signal energy are proposed in [4-6]. However, the selected time-domain features are only suitable for a few specific types of loads. Most references use additional frequency-domain features to detect faults in consideration of misjudgment from the non-linear loads. The frequency-domain transformation algorithms include discrete Fourier transformation and chirp zeta transformation. Discrete Fourier transformation is used most frequently because it can well reflect the frequency-domain features. However, the algorithm could be affected by the determined sampling frequency and observation window. In [7], [8], chirp zeta transformation is proposed to address the issue of poor spectral resolution in Fourier transformation for analyzing the frequency-domain features, and identifies series arc faults based on several low-frequency (LF) harmonic indicators. However, the LF features of arcing current are not obvious in practice and prone to unwanted trips or failure to trip. Discrete wavelet transformation is proposed in [9-12] to carry out hybrid analysis in the time-and-frequency domain. These methods improve the detection accuracy, but they cannot achieve the adaptation of feature thresholds.

Series arc fault detection methods based on machine-learning (ML) algorithms have also been proposed in [13-18]. In [14], a fully connected neural network (FCNN) based on several time-domain and frequency-domain features is used to detect series arc faults. In [15], the particle swarm optimization (PSO) is used to improve the self-organizing feature map (SOM) neural network for detecting faults. Furthermore, support vector machine (SVM) is also used for arc fault

Corresponding author: Yilong Wang (e-mail: 200110002@fzu.edu.cn).

Run Jiang, Guanghai Bao and Yilong Wang are with the College of Electrical Engineering and Automation, Fuzhou University, Fuzhou 350108, China, and also with the Fujian Key Laboratory of New Energy Generation and Power Conversion, Fuzhou 350108, China.

Xiaoqing Gao is with ABB Xiamen Switches Co., Ltd, Second floor, No. 885, Fang Shanxi 2nd Road, Xiamen Torch Hith-tech Zone (Xiang'an) Industrial Zone 361000, China.

Qiteng Hong and Campbell D. Booth are with the Department of Electronic and Electrical Engineering, University of Strathclyde, Glasgow G1 1XW, U.K.

This is a peer-reviewed, accepted author manuscript of the following article: Jiang, R., Wang, Y., Gao, X., Bao, G., Hong, Q., & Booth, C. (2023). AC series arc fault detection based on RLC arc model and convolutional neural network. IEEE Sensors Journal, 23(13), 14618-14627. https://doi.org/10.1109/JSEN.2023.3280009

detection [16]. ML algorithms depend on the classifiers to fit the decision rules between input features and output labels, which solve the problem of threshold adaptation. However, the feature quantities used as the network input highly depend on domain expert experience and cannot satisfy the detection universality in diverse loads. Series arc fault detection algorithms based on convolutional neural network (CNN) have been proposed in [19-20]. These methods do not require researchers to manually extract the fault characteristics, and can learn the characteristics of arbitrary waveform with the help of huge parameter sets of the deep network, thereby achieving high-precision fault classification [21].

Series arc fault detection methods based on statistical analysis and signal processing depend on a large amount of experimental experience and are suitable for relatively small sample systems with the limited load types. In contrast, series arc fault detection methods based on neural network are more suitable for large-scale systems with diverse types of loads. With the help of the nonlinear fitting ability of the network, the detection is not limited to various indicators and fixed thresholds. However, the CNN-based method requires massive data types for training, which brings difficulty to practical applications. Therefore, the existing series arc fault detection methods still have many limitations.

1) For existing loads: different types of loads exhibit different current characteristics, and the same types of loads may also exhibit different current characteristics. Given the current characteristics of various loads, it is necessary to configure a sufficient number of scenarios with different loads and select enough features for detecting the faults. However, the generation of massive real data for training the fault detection algorithms is time-consuming and impractical.

2) For new/unknown loads: series arc fault detection methods are based on the learning of existing loads, neglecting the new features in unknown loads that may be connected to the system. New/unknown load types present challenges to the generalization ability of the detection methods. It is vital to find out the common characteristics of various loads for improving the detection effectiveness under unknown loads.

To cope with the aforementioned limitations, this paper presents a detection method using a novel high-frequency (HF) RLC arc model to drive one-dimensional convolutional neural network (1DCNN). This idea originates from the current transformer used for acquiring differential HF characteristics (D-HFCT) [22-23]. It is found that the D-HFCT can extract the common features: arcing data acquired by the D-HFCT have different types of oscillation features. Different from the traditional features such as shoulder, the common features are not affected by different load types. According to the common features, the RLC-based arc model is developed to generate different types of oscillation signals in consideration of different load types. Then, the 1DCNN is selected as the arc fault detection algorithm, which is trained by massive simulated data. Only one-dimensional time series is used without special processing, and end-to-end arc fault diagnosis is directly realized from data to state results. The experimental results show that the 1DCNN trained by the simulated data can correctly detect series arc faults in practical application. The main works are listed as follows:

1) An improved arc model based on R, L and C is presented to simulate the HF components of arc current.

2) Current with complicated features under different load types is simplified and divided into different types of oscillation signals by the D-HFCT. Since the number of real-data types is limited, the arc model is used for generating different types of oscillation signals to obtain as many samples as possible under various loads.

3) Instead of the limited types of real data, massive and abundant simulated data are used to drive the 1DCNN. Compared with the 1DCNN driven by the limited types of real data, the presented method has good generalization ability under new loads. Furthermore, few references adopt model-driven methods to detect series arc faults in practice. The detection results in this paper indicate that the model-driven methods are also feasible in the field of series arc fault detection.

This paper is organized as follows: Section II shows the HF characteristics of series arc fault current and analyzes their generation process. Furthermore, a new impedance arc model is proposed. Section III presents the implementation of the arc model and its verification in SIMULINK. Section IV introduces a detection algorithm based on the 1DCNN and the simulated data. In Section V, the experimental cases are used for verifying the effectiveness of the proposed detection algorithm. Section VI concludes this paper.

II. Arc Theory and Model

A. High-Frequency Characteristics of Arc Current

As shown in Fig. 1, the D-HFCT is used to collect the HF arc signals and proposed for series arc fault detection. Since the two wires (i.e. the L and N wires) carrying currents in opposite directions weaken the magnetic flux in the magnetic core, the equivalent magnetic flux density in the magnetic core is significantly lower than the saturation magnetic flux density, thus largely mitigating the risk of LF saturation. Furthermore, the gain for HF signals is greater than that for LF signals by the D-HFCT. The arc generator based on the cylindrical copper electrode and the conical carbon electrode is customized according to the standard IEC 62606-2017 [24], and the moving electrode generates an air gap to initiate the arc. The load connector is used to connect different loads. The oscilloscope is used to observe the output voltage waveforms. The line current is acquired by a 1 Ω resistor and compared with the D-HFCT output to show that the D-HFCT signals are more appropriate for series arc fault detection than current signals. The reason is given in the next paragraph.

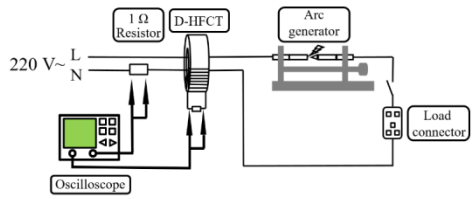

Fig. 1. **Schematic diagram of series arc fault experiment.**

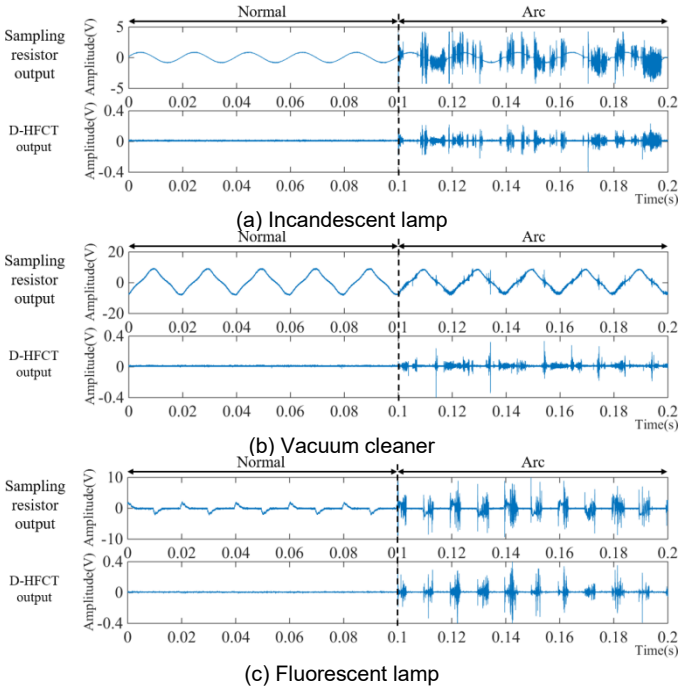

Fig. 2. **Current signals and D-HFCT signals under normal and arc states.**

An incandescent lamp, a vacuum cleaner and a fluorescent lamp are alternately connected to the circuit. The results are shown in Fig. 2. Since the three loads are different, the first waveforms in Fig. 2(a), Fig. 2(b) and Fig. 2(c), respectively, exhibit different characteristics during the arc state, which make arc fault detection difficult. When more new load types are connected to the circuit, there may be new current features, leading to classification failure of the determined detection method. However, with the use of the D-HFCT, its arcing output consistently exhibits different-amplitude HF pulses because the LF features are filtered out. Under the normal state, the output under various loads is uniformly close to zero. Since Gaussian white noise with very small amplitude is unavoidable in the output, the output is not absolutely zero. Therefore, it can be seen that the HF components of arc current are the common features of arc faults.

B. Fundamental Mechanism of HF Arc Current

The air between two separate conductors tends to be insulated. However, when the potential difference between the conductors is above a certain level, the insulated air would be broken down. Then, there would be a high-temperature and conductive object in the air gap, which is often regarded as a series arc fault.

During the breakdown process, the thermal emission and the field emission make many free electrons on the cathode surface enter the gap to generate an arc. The two emissions are generated in different ways. The thermal emission is induced by high temperature when the increased current density at the contact point leads to high temperature. Meanwhile, the distance between the two conductors is very small, which makes the corresponding electric field strength high. Therefore, the field emission is induced by the high electric field strength.

The high electric field strength between the surface protrusion and the arc column tends to induce the formation of the new filed-emission points [25], [26]. However, the heat produced by the arc could vaporize the protrusion, which makes the filed-emission points vanish. The points vanish and regenerate repeatedly, which can constantly provide a large number of electrons to maintain the presence of the arc. The position change between the old points and the new points leads to the movement of the arc root. The continuously moving arc root offers the continuous electron flow to the arc column, which generates the power-frequency (PF) component in the arcing current. The formation and disappearance of the points provide the arc column with intermittent electronic pulses and generate the HF current component.

C. RLC-Based Arc Model

There are very few references that have reported models to simulate the HF arc current. In this paper, an RLC-based arc model has been established. The equivalent circuit diagram is shown in Fig. 3. The impedance arc model is composed of the arc resistance R_a, the arc inductance L_a and the inter-electrode capacitance C_a. During the stable status, the arc is equivalent to a series connection of the low resistance ($R_{a(low)}$) and the arc inductance (L_a). During the arc extinction and regeneration, the arc resistance is equivalent to the high resistance ($R_{a(high)}$). The ideal switches K-K_3 are used to disconnect or connect the main circuit with the arc branches. u_s represents the alternating voltage of the power supply. R_1, L_1 and C_1 represent the equivalent parameters of the power-side line. R_2, L_2 and C_2 represent the equivalent parameters of the load-side line, and Z_L represents the load impedance. The resistance-inductance branch is the LF path of the arc current, and the capacitance branch is the HF path of the arc current.

In the normal operation, K is in the closed state, and K_1-K_3 are in the open state. At this time, the current is mainly determined by the load impedance. When an arc fault occurs, K is always in the disconnected state, and the arc starts to be extinguished and reignited periodically: 1) as shown in Fig. 4(a) and Fig. 4(b), the HF path quickly opens and closes, making the arc current contain HF pulses; 2) as shown in Fig. 4(c), when the arc is extinguished, the arc resistance is very large, and the arc inductance is negligible, which is equivalent to disconnecting K_2 and closing K_1; 3) as shown in Fig. 4(d), when the arc is stable, the arc resistance becomes low, which is equivalent to opening K_1 and closing K_2. The opening and closing of the HF path are random, while the change of the LF path depends on the combustion state of the arc.

The process of the HF path can be regarded as the zero-input response of the second-order circuit, as shown in Fig. 5(a). The operation circuit after the Laplace transform is shown in Fig. 5(b). Assuming that the instantaneous voltage on the power side is U_1, and the instantaneous voltage on the load side is U_2. When the voltage difference is large enough to cause the field-induced breakdown of the HF current emission point, C_1 and C_2 will exchange energy and produce a rapid oscillation process of arc current.

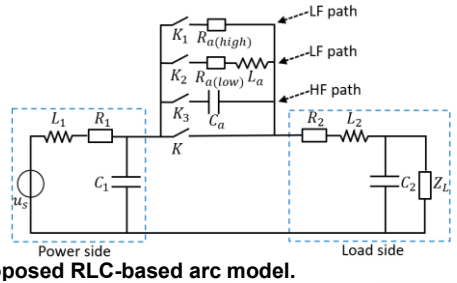

Fig. 3. **Proposed RLC-based arc model.**

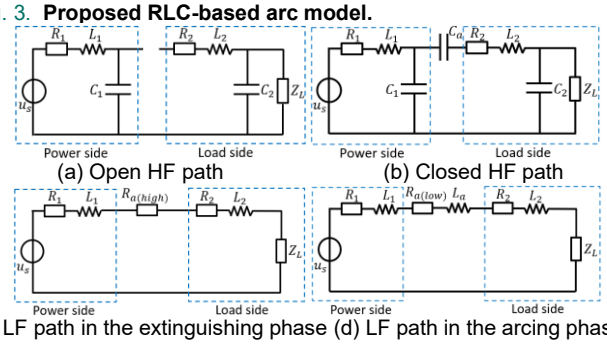

(a) Open HF path (b) Closed HF path

(c) LF path in the extinguishing phase (d) LF path in the arcing phase

Fig. 4. **Equivalent circuits at different stages.**

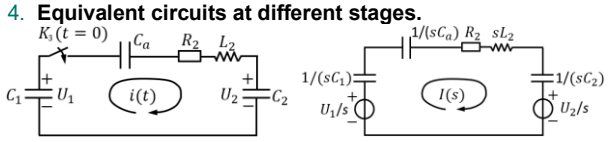

(a) Zero-input response circuit (b) Operation circuit

Fig. 5. **Analysis of HF-path process.**

The equation is listed as follows by the loop current method:

$$[R_2 + sL_2 + (\frac{1}{sC_1} + \frac{1}{sC_2} + \frac{1}{sC_a})]I(s) = \frac{U_1 - U_2}{s} \quad (1)$$

Then, the frequency-domain solution I(s) can be derived as:

$$I(s) = \frac{U_1 - U_2}{L_2 s^2 + R_2 s + C} \quad (2)$$

where $C = (C_1C_a + C_2C_a + C_1C_2)/C_1C_2C_a$. In fact, the pulse of HF arc current exhibits attenuated oscillation, and the circuit is in an under-damped state, so the time domain solution of the current can be obtained:

$$i(t) = \frac{U_1 - U_2}{\omega L_2} e^{-\alpha t} sin(\omega t),\ \omega = \sqrt{1/L_2C - (R_2/2L_2)^2}\ and\ \alpha = R_2/2L_2 \quad (3)$$

where ω is the angular frequency, and α is the damped coefficient of damped oscillation. The HF characteristics of arc current are related to arc voltage, arc parameters, and line parameters. They mainly depend on the HF charging and discharging process of ground capacitance through arc capacitance and line impedance.

III. Simulation Verification of Arc Model

To verify the effectiveness of the proposed arc model, the detailed simulation is shown in Fig. 6 and Fig. 7. Fig. 6 divides the circuit into the LF and HF paths, which are used to generate LF and HF components, respectively. The arc controller of Fig. 6 is related to Fig. 7(a) and determines whether the components are normal or arcing. In the normal state, K is closed, and K_4 is disconnected. The LF path is short-circuited, and the HF path is disconnected. When a fault occurs, K is disconnected. Then, K_4 is closed, and both the LF path and the HF path begin to work. For the LF path, whether R_a is high or low depends on the arcing state, which is shown in Fig. 7(c). For the HF path, the corresponding switch K_3 is randomly switched on and off at a high speed. In the simulation, by setting the signal generation probability of the binary sequence generator, the opening and closing of K_3 are random, as shown in Fig. 7(b). In order to improve the simulation effect, Gaussian white noise is added to the simulated signal. Finally, the HF, LF and white-noise components can be put together to represent the line current i.

Resistive loads with working current of 1 A, 2 A and 5 A, respectively, are used to verify the effectiveness of the arc model. For comparison, the simulated output current has been converted to the voltage by the sensor. The simulated and actual results are shown in Fig. 8. In the normal state, the HF signals are close to zero. In the arc state, a large number of HF spikes appear in the signals. As the load resistance decreases, the HF components of the arc will slightly decrease. The simulated waveform of Fig. 8(b) retains the fault characteristics of the actual load waveform of Fig. 8(a). This can prove the validity of the arc model. It is possible to generate enough HF arc current data for training the neural network by traversing the initial phase angle of the AC power source, the frequency of the Bernoulli random sequence and the load type.

IV. Deep Learning Detection Algorithm

CNN is composed of multiple network layers connected in series. The standard CNN [27] usually consists of an input layer, multiple convolutional-and-pooling layers, one or two fully connected layers and an output layer. The structure of the 1DCNN model proposed in this paper is shown in Fig. 9. The input layer is used to receive a 1D array composed of raw D-HFCT signals. The output layer is used to output the final results. Hidden layers consist of convolutional layers, pooling layers and fully connected layers, and are used for feature recognition. The hidden layers represent a complex nonlinear mapping from the input layer to the output layer, and fit the decision rule between the input data and the output data.

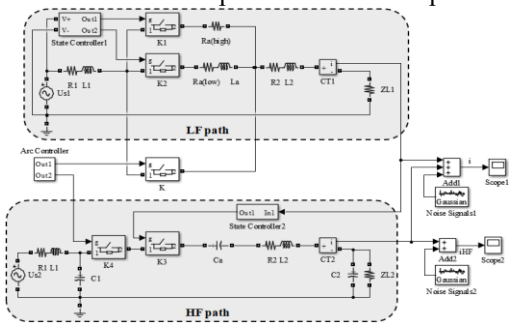

Fig. 6. **Simulated-circuit diagram of impedance arc model.**

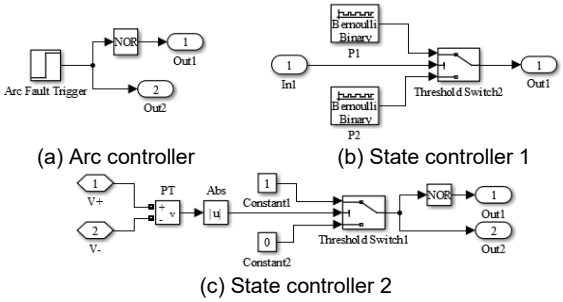

(a) Arc controller (b) State controller 1

(c) State controller 2

Fig. 7. **Arc control module.**

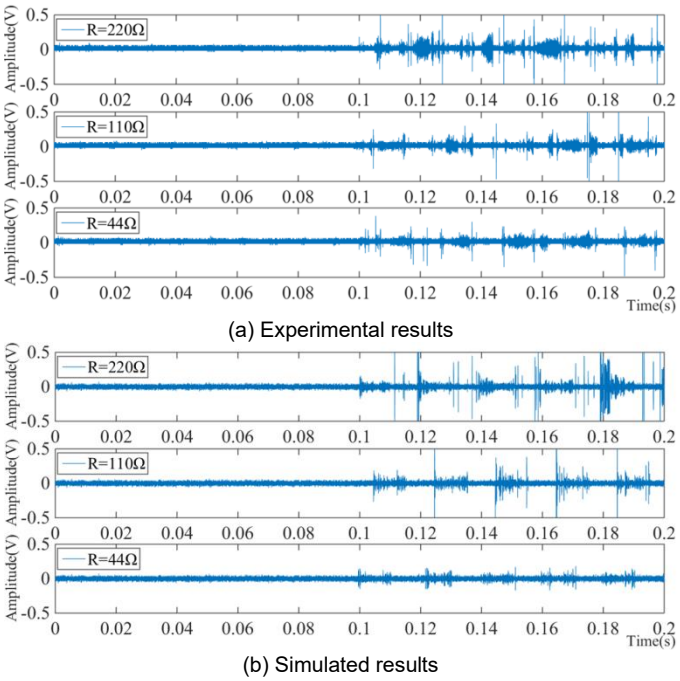

(a) Experimental results

(b) Simulated results

Fig. 8. **HF features of experimental results and simulated ones.**

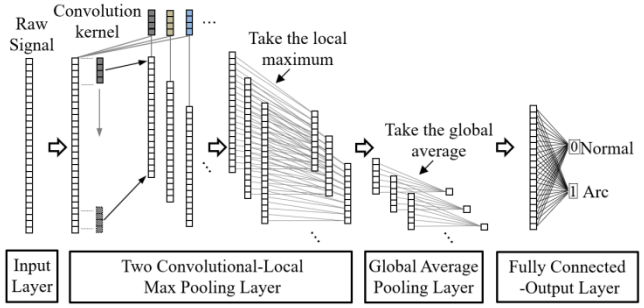

Fig. 9. **Structure of the proposed 1DCNN.**

The convolutional layers extract the features of the sequence through different convolutional kernels (filters) acting on the original sequence, and different convolutional kernels extract different features. Each convolutional layer has several convolution kernels, and the specific parameters of these convolutional kernels are adaptively learned by the training process. The convolution-calculation output can be obtained as:

$$Y = f(X * w + b) \tag{4}$$

where X and Y are the input column vector and the output matrix of the first convolutional layer, respectively. The input data are normalized before being input into the first convolutional layer. The magnitude of all the data is scaled to [-1, 1], which can speed up the network convergence and avoid the problem of gradient disappearance or explosion caused by excessive numerical differences. w and b represent the weight vector and the offset vector, respectively. * represents the discrete convolution operation. f is the nonlinear activation function, which realizes the nonlinear mapping from input to output. The rectified linear unit (ReLU) [28] with faster convergence speed is selected, and its formula is:

$$f = \max(0, x) \tag{5}$$

The pooling layers do not contain trainable parameters, but they calculate the average or maximum value of the data segment according to the specified step size. Max pooling is the most common. It is equivalent to distilling the input data and simplifying the information from the convolutional layers while ensuring the same signal characteristics. After passing through the pooling layer, the processed data should be input into several fully connected layers for classification. However, there are a so large number of parameters in the fully connected layers that the model becomes very large. The number of model parameters can be greatly reduced by using the global average pooling layers instead of the fully connected layers.

The fully connected layers follow two steps. Firstly, the 1D column vector output from the global average pooling layers is mapped to two numerical values, representing the original output of the fully connected layers. This mapping relies on the weight and bias between the input neuron group and each output, and the operation is as follows:

$$\begin{cases} y_0 = w_0^T x + b_0 \\ y_1 = w_1^T x + b_1 \end{cases} \tag{6}$$

where y_0 and y_1 are the original output of the fully connected layers. x is the input column vector of the input neurons. ${w_0}^T$ and ${w_1}^T$ are the weight matrices between the input neurons and the two output neurons. b_0 and b_1 represent the offset of the two output neurons, respectively. Secondly, the Sigmoid function is selected as the activation function, and the two numerical values are mapped between 0 and 1. The calculation formula of classification probability is:

$$\begin{cases} P_0 = e^{y_0} / (e^{y_0} + e^{y_1}) \\ P_1 = e^{y_1} / (e^{y_0} + e^{y_1}) \end{cases} \tag{7}$$

The two mapping values P_0 and P_1 represent the probability of the normal state (label 0) and the arc state (label 1), respectively, and the relatively large probability value is taken as the final classification result.

V. Experimental Verification

A. Series Arc Fault Experimental Setup

In this work, a detection scheme that combines the simulated data and the 1DCNN has been established and used to detect series arc faults under real loads. The experimental setup is shown in Fig. 10. The deep learning model is developed using Python & Pycharm on a laptop equipped with an AMD Ryzen 4800H CPU and a 16 GB RAM. The training and the validation of the 1DCNN model depend on the data generated by the arc model. The real signals collected by the D-HFCT are used to further evaluate the generalization ability of the trained 1DCNN. In the normal state, the simulated data containing small amplitude Gaussian white noise construct normal samples by slicing every two cycles. The length of each sample is 0.04 s, and the number of sampling points is 16000. The simulated data in the arc state follow the same steps. Before training the 1DCNN, the samples must be labeled as 0 in the normal state and 1 in the arc state. The original set containing 5000 samples is constructed, and these samples are evened out between the two states. 4000 samples are randomly selected as the training set, and the remaining 1000 samples are used as the validation set.

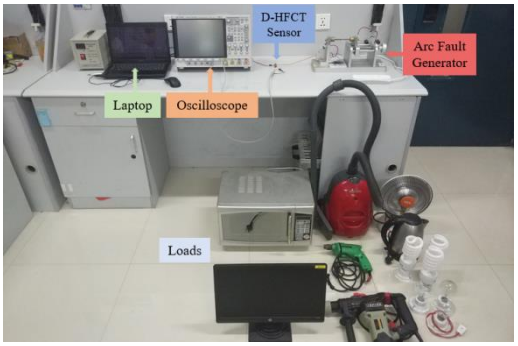

Fig. 10. **Experimental setup.**

B. Network Structure of 1DCNN Model

The network structure of the 1DCNN model established in this paper is shown in Table I. The "Reshape" layer normalizes the original data and performs row-column conversion to dock with the convolutional layers. The convolution operation is used to extract features, and the number of convolution layers and filters is decreased as much as possible to reduce computation cost and parameter number. Additionally, the "Max Pooling" layers with relatively large size and stride are used, and the Global Average Pooling replaces the fully connected layers (Dense) to further reduce computation cost and parameter number. The related hyper-parameters are determined through experiments.

At each training epoch, the training set trains the network in batches to adjust the network parameters. At the end of each epoch, the network performance is tested with the validation set. The changes of loss and accuracy in the training and the validation, respectively, are shown in Fig. 11. The maximum training epoch is set as 100. When running to the 10th epoch, the network has shown less loss and higher accuracy, which are a good result. The network parameter configuration is saved by using the callback function when the validation loss is minimal.

TABLE I
NETWORK STRUCTURE OF 1DCNN MODEL

Layer	Hyper-parameter	Output
Reshape	-	(16000,1)
Conv 1	5/50/2(num/size/stride)	(7976,5)
Max Pooling 1	50/50(size/stride)	(159,5)
Conv 2	10/25/2(num/size/stride)	(80,10)
Max Pooling 2	25/25(size/stride)	(3,10)
Global Average Pooling	-	10
Dense	-	2

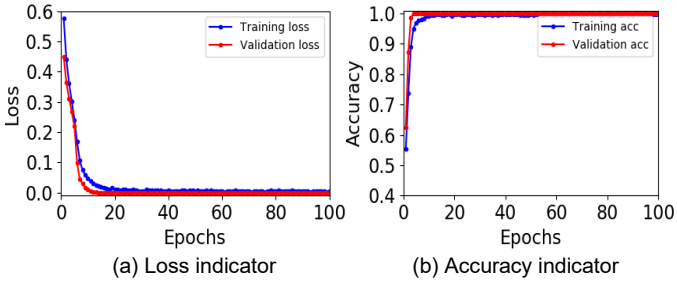

(a) Loss indicator (b) Accuracy indicator

Fig. 11. **Iteration process of training and validation.**

C. Actual Detection Case

The real samples are put into the trained 1DCNN, including a normal sample and an arcing sample. The output of different network layers is visualized to show the detection process, which is shown in Fig. 12, Fig. 13, Table II, and Table III. As can be seen from Fig. 12(c) and Fig. 13(c), the output of the Conv 1-layer contains almost all the information of the original waveform, and its input is the normalized waveform of Fig. 12(a) and Fig. 12(b). Due to the ReLU function, the output only displays the waveform whose values are larger than zero. After the pooling layer, the signal becomes sparse, but the overall trend of the waveform is still maintained. Due to the lack of spikes in Fig. 12(d), the waveforms filtered by Conv 2-3, Conv 2-6, Conv 2-9 and Conv 2-10 are almost zero, as shown in the 3rd, 6th, 9th and 10th waveforms of Fig. 12(e), respectively. On the contrary, there are many spikes in Fig. 13(d). The waveforms filtered by Conv 2-3, Conv 2-6, Conv 2-9 and Conv 2-10 also contain spikes, as shown in Fig. 13(e). Therefore, the difference between the normal sample and the arcing sample becomes obvious after the Conv 2-layer, and the waveforms filtered by the four convolutional filters are the most noticeable.

Subsequent layer output is given in Table II and Table III. After the Max Pooling (M-P 2) layer and the Global Average Pooling (G-A-P) layer, the data dimension becomes 1D, and the waveform becomes a column vector with a length of 10. The table gives the weight and the bias of the Dense layer. According to the equation (6), two values can be obtained, which are the original output of the Dense layer. Then, the values are converted into two probabilities according to the equation (7). As can be seen from Table II, the probability that the normal sample is classified into the normal state (label 0) is 1, and the probability of being classified into the arc state (label 1) is 0. On the contrary, as can be seen from Table III, the probability that the arcing sample is classified into the arc state (label 1) is 1, and the probability of being classified into the normal state (label 0) is 0. Therefore, the 1DCNN trained by the simulated data can identify normal and arcing signals accurately.

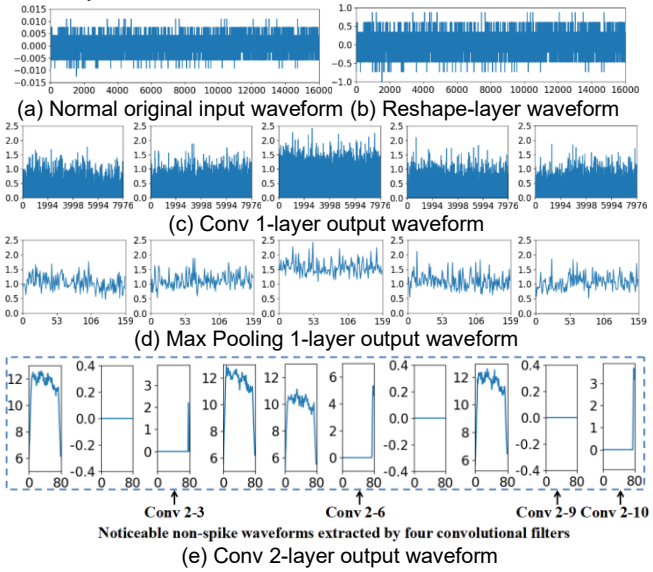

Fig. 12. **Network visualization of a normal sample.**

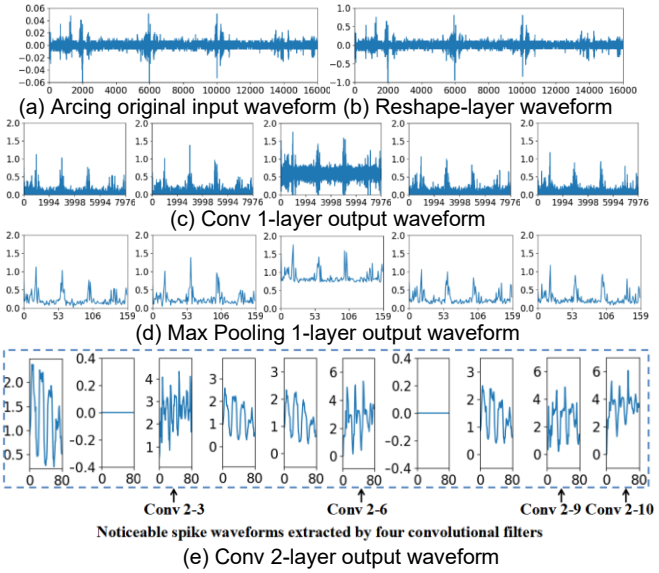

Fig. 13. **Network visualization of a fault sample.**

D. Arc Fault Detection Strategy

The detection process is shown in Fig. 14. The actual data with a length of 1 s are cut into 25 data segments (samples) by a two-cycle (0.04 s) step, and the number of data segments classified into the arc state is counted. There are 9 types of common household loads used to generate the test data. In Table IV, these loads are unknown for the trained 1DCNN because only the oscillation signals generated by the arc model are used to train the 1DCNN. The proposed detection algorithm achieves 100% accuracy in some resistive and nonlinear loads, and more than 96% accuracy in inductive loads. This is mainly because the carbon brushes and commutators of the motor in inductive loads generate commutation sparks, leading to some misjudged samples. However, thanks to the continuous detection strategy, the misjudged samples would not lead to the final misjudgment. The continuous detection means that series arc faults will be recognized as long as there are at least N_{thre} arcing data segments among 25 data segments. Only when the number of data segments classified into the arc state is 7 or more ($N \geq 7$), it is considered as a real arc fault. When N_{thre} is smaller than 7, the misjudgment would occur sometimes because of the misjudged samples. Therefore, N_{thre} is selected as 7. Furthermore, it can also avoid the misjudgment from the starting process of loads.

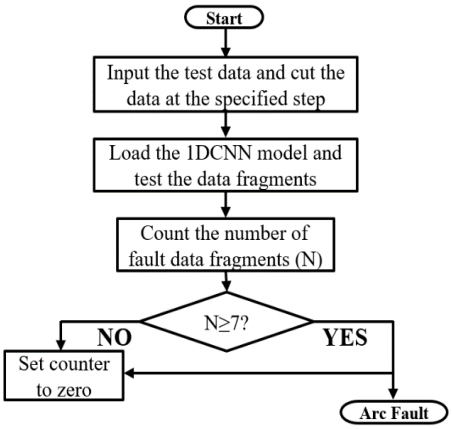

Fig. 14. **Flow chart of series arc fault detection.**

TABLE II
PARTIAL LAYER OUTPUT (REAL NORMAL SAMPLE)

M-P 2 output	G-A-P Output	Dense Wight	Dense Bias	Dense output	P_0/P_1
12.502517 12.581809 12.150744	12.41169	0.586779 -0.703849			
0 0 0	0	0.286219 -0.197791			
0 0 0	0	-0.670362 1.04945			
12.874266 12.639414 12.181286	12.564988	0.571263 -0.63562			
10.703744 11.106236 10.730649	10.846877	0.793833 -0.79623	-0.24451 0.190474	30.63986 -32.7399	1 0
0 0 0	0	-0.90857 0.802369			
0 0 0	0	0.292806 -0.525038			
12.337868 12.594505 12.009651	12.314008	0.634475 -0.614848			
0 0 0	0	-0.84312 0.954623			
0 0 0	0	-0.806546 0.696096			

TABLE III
PARTIAL LAYER OUTPUT (REAL FAULT SAMPLE)

M-P 2 output	G-A-P Output	Dense Wight	Dense Bias	Dense output	P_0/P_1
2.3714936 2.2549934 1.9275188	2.1846685	0.586779 -0.703849			
0 0 0	0	0.286219 -0.197791			
4.061629 4.3071294 3.7570655	4.041941	-0.670362 1.04945			
2.5691764 2.2164252 1.9750535	2.2535517	0.571263 -0.63562			
2.3297687 2.24926 1.8570101	2.1453464	0.793833 -0.79623	-0.24451 0.190474	-9.97264 10.43709	0 1
4.91534 5.0860634 5.348719	5.1167073	-0.90857 0.802369			
0 0 0	0	0.292806 -0.525038			
2.4929726 2.3851748 1.9757875	2.2846448	0.634475 -0.614848			
4.6217356 4.8606567 3.719809	4.400734	-0.84312 0.954623			
5.287821 4.9507236 6.0576763	5.4320736	-0.806546 0.696096			

To further show the main contributions of the presented detection method, Table V lists advantages and disadvantages between the presented method and the published methods. Reference [4] mainly uses the signal energy to detect faults. The indicator is simple and easy to be implemented. However, the threshold changes in some nonlinear loads. The design of features and thresholds should be reconsidered.

TABLE IV
ARC FAULT DETECTION RESULT UNDER ACTUAL NEW LOAD

Load	Normal Size/Result	Arc Size/Result	Average Accuracy
Incandescent lamp	100/100	100/100	100%
Electric kettle	100/100	100/100	100%
Electric heater	100/100	100/100	100%
Electric drill	100/92	100/108	96%
Electric hammer	100/97	100/103	98.5%
Vacuum cleaner	100/99	100/101	99.5%
Computer screen	100/100	100/100	100%
Fluorescent lamp	100/100	100/100	100%
Microwave oven	100/100	100/100	100%

TABLE V
COMPARISON WITH EXISTING SERIES ARC FAULT DETECTION METHOD

Reference	Detection method	Contribution	Disadvantage
[4]	Singular value decomposition and reconstruction + signal energy	• Simple feature • High detection accuracy	Threshold change in nonlinear loads
[16]	Support vector machine based on time-domain difference energy, etc. + FFT-based harmonic analysis (PCA processing)	• Low-dimensional feature vector • High detection accuracy	Only suitable for a few load types
[20]	Raw current signal-based convolutional neural network	• Without additional signal processing • High detection accuracy	Not suitable for new load types
[29]	Machine-learning methods based on many Time-domain and frequency-domain features	• Arc fault detection + load type classification	Fair detection accuracy
Presented method	Simulated HF arc model-based convolutional neural network	• Without additional signal processing • High detection accuracy • Suitable for new load types • Convenient training by new arc model /real data not required	-

Reference [16] and [29] combine the time-domain features with the frequency-domain features to detect faults. They are suitable for a few load types, and the detection accuracy would decrease with the increase of load types. Reference [20] adopts raw current signal-based CNN to detect faults and achieves high detection accuracy when the training set is sufficient, but the detection accuracy would drop under new load types. The presented method has good detection accuracy under many new loads because it is driven by abundant types of oscillation signals and takes account of as many signal types as possible. There are also other methods for generating the simulated data, such as physics-based models and data augmentation. However, the physics-based models tend to be time-consuming, while the data augmentation cannot take into account different combinations of circuit parameters. Furthermore, the quality of data generated by the data augmentation depends on the quality and diversity of the original data. Therefore, it is recommended to use the equivalent circuit models. However, high-frequency current features cannot be recovered by the traditional arc models, such as Mayr model, Cassie model and so on. Given the limitations of these arc models, an improved arc model based on RLC is presented to more accurately generate data.

In terms of computation cost and parameters, the complexity of the standard 1DCNN is $N_1k_1c_0c_1+\cdots+N_tk_tc_{t-1}c_t+N_tc_tm_1+m_{s-1}m_s+2m_s$ for binary classification, where N_t, k_t and c_t are the feature-map size, the filter size and the filter number, respectively, in the t-th convolutional layer, and m_s is the neuron number of the s-th layer in neural network. To reduce the complexity, the Global Average Pooling is used instead of the neural network in Section V, and the overall complexity is expressed as $N_1k_1c_0c_1+\cdots+N_tk_tc_{t-1}c_t+N_tc_t+2c_t$. In Section V, the layer number, the filter number and the feature-map size are also decreased to reduce the complexity without compromising the detection accuracy.

VI. CONCLUSION

To improve the detection accuracy under unknown load types, this paper has presented a 1DCNN method driven by an improved arc model. The D-HFCT used in this paper proves that the HF oscillation features are common in arcing current, and the signals acquired by the D-HFCT can be divided into different oscillation types. To simulate the HF arcing features, the improved arc model is composed of the arc resistance, the arc inductance and the arc capacitance. Since the types of real data are limited, the improved arc model is used to generate various types of oscillation signals by adjusting the initial phase angle, the Bernoulli-sequence frequency and the load resistance. Then, the simulated data are used to drive the 1DCNN, and the trained 1DCNN is tested under various real loads. Finally, the presented method achieves high detection accuracy under 9 types of commonly used appliances, whose data are not used to train the 1DCNN. Compared with the published methods, the presented method is more suitable to detect series arc faults under unknown loads. Based on series arc fault detection, the future work will be focused on fault location to isolate fault inception points correctly.

REFERENCES

[1] W. Miao, Q. Xu, K. H. Lam, P. W. T. Pong and H. V. Poor, "DC Arc-Fault Detection Based on Empirical Mode Decomposition of Arc Signatures and Support Vector Machine," *IEEE Sensors J.*, vol. 21, no. 5, pp. 7024-7033, March 2021.

[2] T. Zhang, R. Zhang, H. Wang, R. Tu and K. Yang, "Series AC Arc Fault Diagnosis Based on Data Enhancement and Adaptive Asymmetric Convolutional Neural Network," *IEEE Sensors J.*, vol. 21, no. 18, pp. 20665-20673, Sept. 2021.

[3] Z. Wang, C. Han, H. Gao and F. Guo, "Identification of Series Arc Fault Occurred in the Three-Phase Motor With Frequency Converter Load Circuit via VMD and Entropy-Based Features," *IEEE Sensors J.*, vol. 22, no. 24, pp. 24320-24332, Dec. 2022.

[4] R. Jiang, G. Bao, Q. Hong and C. D. Booth, "A Coupling Method for Identifying Arc Faults Based on Short-Observation-Window SVDR," *IEEE Trans. Instrum. Meas.*, vol. 70, pp. 1-10, 2021, Art no. 3513810.

[5] J. Jiang, W. Li, Z. Wen, Y. Bie, H. Schwarz and C. Zhang, "Series Arc Fault Detection Based on Random Forest and Deep Neural Network," *IEEE Sensors J.*, vol. 21, no. 15, pp. 17171-17179, Aug. 2021.

[6] M. Ahmadi, H. Samet, and T. Ghanbari, "A new method for detecting series arc fault in photovoltaic systems based on the blind-source separation," *IEEE Trans. Ind. Electron.*, vol. 67, no. 6, pp. 5041–5049, Jun. 2020.

[7] G. Artale, A. Cataliotti, V. Cosentino, D. D. Cara, S. Nuccio, and G. Tinè, "Arc fault detection method based on CZT low-frequency harmonic

current analysis," *IEEE Trans. Instrum. Meas*., vol. 66, no. 5, pp. 888–896, May 2017.

[8] G. Artale, A. Cataliotti, V. Cosentino, S. Nuccio, D. D. Cara, G. Tinè, and G. Privitera, "A set of indicators for arc faults detection based on low frequency harmonic analysis," in *Proc. IEEE Int. Instrum. Meas*. Technol. Conf. pp. 1183–1188, May. 2016.

[9] D. A. Asfani, D. Fahmi, I. M. Y. Negara, and I. G. N. S. Hernanda, "Low-voltage arcing detection on non-linear load with total harmonic distortion and power factor variations," in *Proc. Int. Seminar Intel. Tech. Appl.*, pp. 265–269, Aug. 2019.

[10] J. Hong-Keum et al., "Extraction of series arc signals based on wavelet transform in an indoor wiring system," *Trans. Electr. Electron. Mater*., vol. 18, no. 4, pp. 221–224, Aug. 2017.

[11] Z. D. Yin, L. Wang, Y. J. Zhang, and Y. Gao, "A novel arc fault detection method integrated random forest, improved multi-scale permutation entropy and wavelet packet transform," *Electronics*, vol. 08, no. 4, pp. 396, Apr. 2019.

[12] Q. Pan, J. Slavisa, L. Jinmi, and S. Patrick, "Discrete wavelet transform optimal parameters estimation for arc fault detection in low-voltage residential power networks," *Elect. Power Syst. Res.*, vol. 143, pp. 130–139, Feb. 2017.

[13] W. Li, A. Monti, and F. Ponci, "Fault detection and classification in medium voltage DC shipboard power systems with wavelets and artificial neural networks," *IEEE Trans. Instrum. Meas*., vol. 63, no. 11, pp. 2651–2665, Nov. 2014.

[14] Y. K. Wang, F. Zhang, X. H. Zhang, and S. W. Zhang, "Series AC arc fault detection method based on hybrid time and frequency analysis and fully-connected neural network," *IEEE Trans. Ind. Inf*., vol. 15, no. 12, pp. 1–10, Dec. 2019.

[15] N. Qu, J. T. Chen, J. K. Zuo, and J. H. Liu, "PSO-SOM neural network algorithm for series arc fault detection," *Adv. Math. Phys*., vol. 2020, pp. 1–8, Jan. 2020.

[16] J. Jiang, Z. Wen, M. X. Zhao, Y. F. Bie, C. Li, M. G. Tan, and C. H. Zhang, "Series arc detection and complex load recognition based on principal component analysis and support vector machine," *IEEE Access*, vol. 7, pp. 47221–47229, Mar. 2019.

[17] N. Qu, J. H. Wang, and J. H. Liu, "An arc fault detection method based on current amplitude spectrum and sparse representation," *IEEE Trans. Instrum. Meas.*, vol. 68, no. 10, pp. 3785–3792, Oct. 2019.

[18] Y. K. Wang, F. Zhang, and S. W. Zhang, "A new methodology for identifying arc fault by sparse representation and neural network," *IEEE Trans. Instrum. Meas*., vol. 67, no. 11, pp. 2526–2537, Nov. 2018.

[19] K. Yang, R. B. Chu, R. C. Zhang, J. C. Xiao, and R. Tu, "A novel methodology for series arc fault detection by temporal domain visualization and convolutional neural network," *Sensors*, vol. 20, no. 1, pp. 162, Jan. 2020.

[20] Y. Wang et al., "ArcNet: Series AC Arc Fault Detection Based on Raw Current and Convolutional Neural Network," *IEEE Trans. Ind. Informat*., vol. 18, no. 1, pp. 77-86, Jan. 2022.

[21] G. W. Xu, M. Liu, Z. F. Jiang, W. M. Shen, and C. X. Huang, "Online fault diagnosis method based on transfer convolutional neural networks," *IEEE Trans. Instrum. Meas*., vol. 69, no. 2, pp. 509–520, Feb, 2020.

[22] G. H. Bao, X. Q. Gao, R. Jiang, and K. Huang, "A novel differential high-frequency current transformer sensor for series arc fault detection," *Sensors*, vol. 19, no. 17, pp. 3649, Aug. 2019.

[23] G. H. Bao, R. Jiang, and X. Q. Gao, "Novel series arc fault detector using high-frequency coupling analysis and multi-indicator algorithm," *IEEE Access*, vol. 7, pp. 92161–92170, Jul. 2019.

[24] General requirements for arc fault detection devices, IEC 62606, International Electrotechnical Commission: Geneva, Switzerland, 2017.

[25] J. J. Shea, and X. Zhou, "RF currents produced from AC arcs with asymmetrical electrodes," in *Proc. 56th IEEE Holm Conf. Elect. Contacts*, pp. 188–198, Oct. 2010.

[26] J. J. Shea, and J. B. Carrodus, "RF current produced from electrical arcing," in *Proc. 57th IEEE Holm Conf. Elect. Contacts*, pp. 1–9, Sep. 2011.

[27] O. Abdeljaber, O. Avci, M. S. Kiranyaz, B. Boashash, H. Sodano, and D. J. Inman, "1-D CNNs for structural damage detection: Verification on a structural health monitoring benchmark data," *NeuroComputing*, vol. 275, pp. 1308-1317, Jan. 2017.

[28] K. Alex, S. Ilya, and E. H. Geoffrey, "ImageNet Classification with Deep Convolutional Neural Networks," in *Proc. Neural Information Processing Systems*, vol. 25, 2012.

[29] N. Qu, J. Zuo, J. Chen and Z. Li, "Series Arc Fault Detection of Indoor Power Distribution System Based on LVQ-NN and PSO-SVM," *IEEE Access*, vol. 7, pp. 184020-184028, Dec. 2019.